Chapter 4

MULTISTEP ELECTRON TRANSFER: "HOPPING MAPS" TUTORIAL AND APPLICATION

Portions of this work are excerpted with permission from:

J. J. Warren, M. E. Ener, A. Vlček Jr., J. R. Winkler, H. B. Gray.
Coord. Chem. Rev. **2012**, *256*, 2478-2487.

4.1. Electron transfer through proteins

Biological energy conversions are critical for cellular function. Photosynthesis harnesses the energy from sunlight to generate reactive chemical bonds in adenosine triphosphate (ATP) and reduced nicotinamide adenine dinucleotide (NADH).[1,2] Cellular respiration generates those same species using energy stored in the chemical bonds of sugars (glucose).[3,4] These complex reactions are carried out by an intricate network of membrane-bound multi-protein systems (**Figure 4.1**). More than 10 individual electron transfer (ET) steps take place during the catalysis that couples ATP and NADH synthesis to the oxidation of water (photosynthesis) or the reduction of O_2 (respiration).

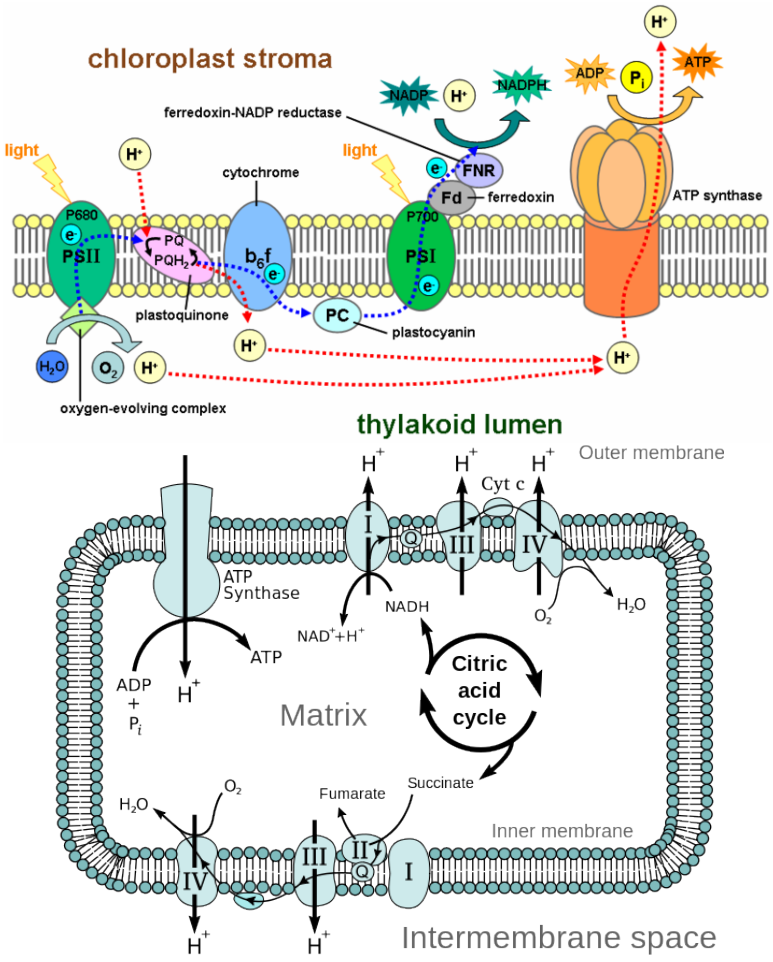

Figure 4.1. Multistep ET in biological energy conversion systems. **Top**: Photosynthetic reaction scheme. **Bottom**: Aerobic respiration in mitochondria.

A simpler energy conversion system was discussed in Chapters 2 and 3; light energy (a laser pulse) was used to generate the high-valent compound II (CII) in Ru photosensitizer–cytochrome P450 conjugates by oxidizing a water molecule bound to the heme. Even within this artificial system, as many as four individual ET events maybe contribute to CII formation (**Figure 4.2**): ET quenching of the $^{*}Ru^{II}$ excited state to form Ru^{III}, transient oxidation of tryptophan96, hole transfer to the porphyrin ring, and hole transfer to the iron center.

In all of these systems, native and artificial, electrons and holes must be rapidly and efficiently separated, and transported across many-angstrom distances. Recombination of these electron-hole pairs would result in nonproductive loss of energy as heat, without accomplishing the desired reactions. For examples of scale, the width of a membrane lipid bilayer can span be 30 Å or more,[5] and the Ru-Fe distance in Ru-P450 conjugates is 24 Å.

In order to address these complex, multi-ET processes, we must first understand the factors that govern single-step ET within simple systems (e.g., small, model proteins). We then can asses how enzymes use multiple, short ET steps (electron "hopping") to rapidly transport charges over biologically-relevant distances.

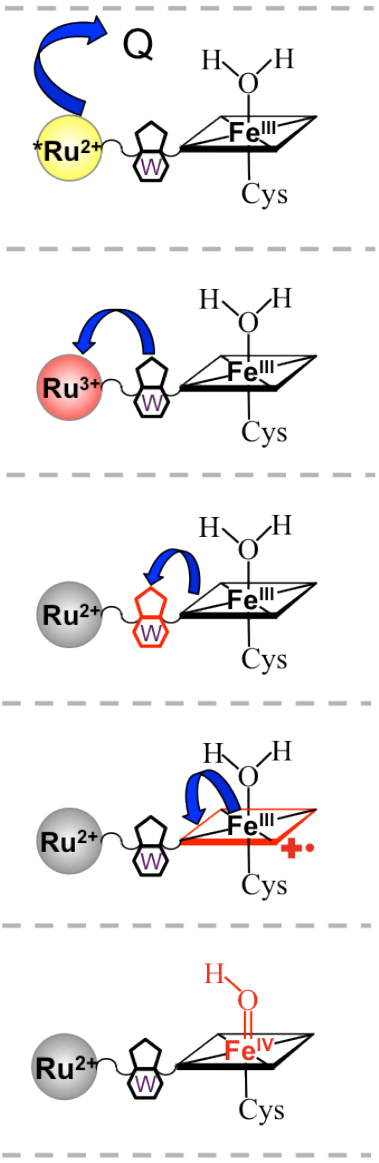

Figure 4.2. Sequential ET steps in the photo-triggered oxidation of Ru-P450 conjugates. Blue arrows represent individual ETs. Oxidized species are colored red. Q is an exogenous quencher.

Method for examining ET in proteins: photochemical triggering

The Gray group and others have spent decades studying fundamental aspects of ET within proteins by tethering inorganic photosensitizers to protein surfaces (**Figure 4.3**). As mentioned for Ru-P450 conjugates, laser pulses trigger ET between the photosensitizer excited (or quenched) state, and a redox active center

within the protein. Redox active centers include copper in *Pseudomonas aeruginosa* azurin,[6–9] heme iron in cytochrome *c*,[10–13] and also amino acid side chains within complex enzymes such as ribonucleotide reductase (the enzyme that deoxygenates nucleotides, necessary for DNA, **Figure 4.4**).[14] By varying the nature and location of the tethered photosensitizer, as well as the composition of the intervening protein, the effects of distance, driving force, and biological medium can be examined.[6,13] These studies and others have shown that ET events through biological media can be analyzed using semiclassical ET theory.

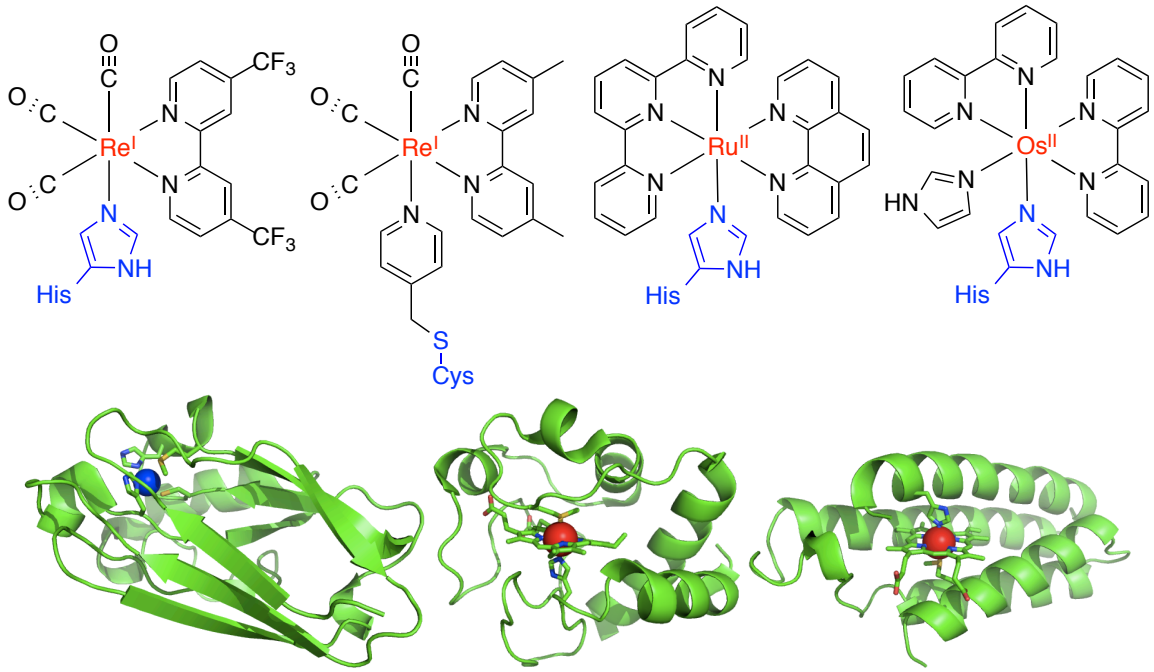

Figure 4.3. Photosensitizers and metallo-proteins. **Top**: A variety of photosensitizers tethered to amino acids. **Bottom**: redox active model proteins. Left to right: *P. aeruginosa* azurin (PDB: 1JZG, Cu in blue), horse heart cytochrome c (PDB: 1HRC, heme Fe in red), cytochrome b562 (PDB: 256B, heme Fe in red). All images of protein crystal structures in this Chapter were made using PyMol graphics software for Mac.

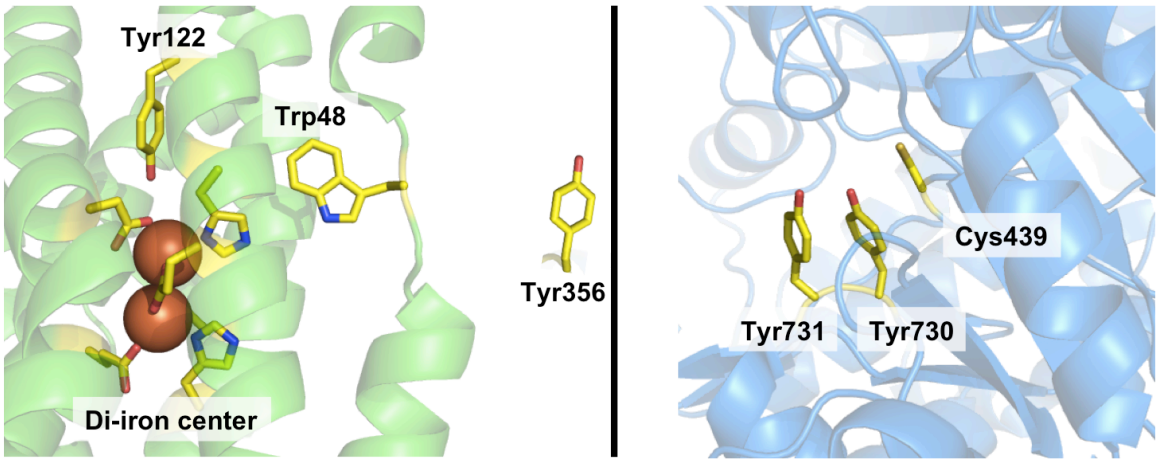

Figure 4.4. Ribonucleotide reductase from *E. coli*. Amino acid side chains along an ET path between Tyr122 radical-initiation and Cys439 active site (alpha, R1 subunit: blue, PDB 1RLR; beta, R2 subunit: green, PDB 1MRX).

This Chapter first offers a basic description of the theoretical underpinnings required for analyzing single-step ET, and some of the conclusions that have come out of single-step analysis in biological systems. This is followed by extension of electron tunneling to describe electron hopping, with a discussion of biochemical systems that employ this mechanism. We describe the step-by-step generation of a "hopping map," a plot of multistep ET rate dependence on driving force for the first and overall reaction steps. We examine the utility of the hopping map for analyzing photo-triggered two-step hopping in rhenium-labeled azurin, and draw some general conclusions from this reactivity. We address some of the challenges and limitations of this type of analysis, and discuss the applicability to native ET systems. Finally, we address the utility of this hopping analysis for multistep ET in ruthenium-labeled cytochrome P450 (Chapters 2 and 3).

4.2. Single-step electron tunneling: semiclassical theory

We will begin examining ET reactions using semiclassical theory. ET between an electron/hole donor (D) and an acceptor (A) can be described using two harmonic

potential energy surfaces (**Figure 4.5**), where the positions along the horizontal axis describe nuclear configurations and geometries, and the vertical axis describes the system's free energy. The parabolic surface on the left (red) describes the reactant state in which the electron or hole (denoted as a dot) resides on the donor moiety: (D•|A). The right surface (blue) describes the product state, in which the electron/hole has been transferred to the acceptor (D|A•).

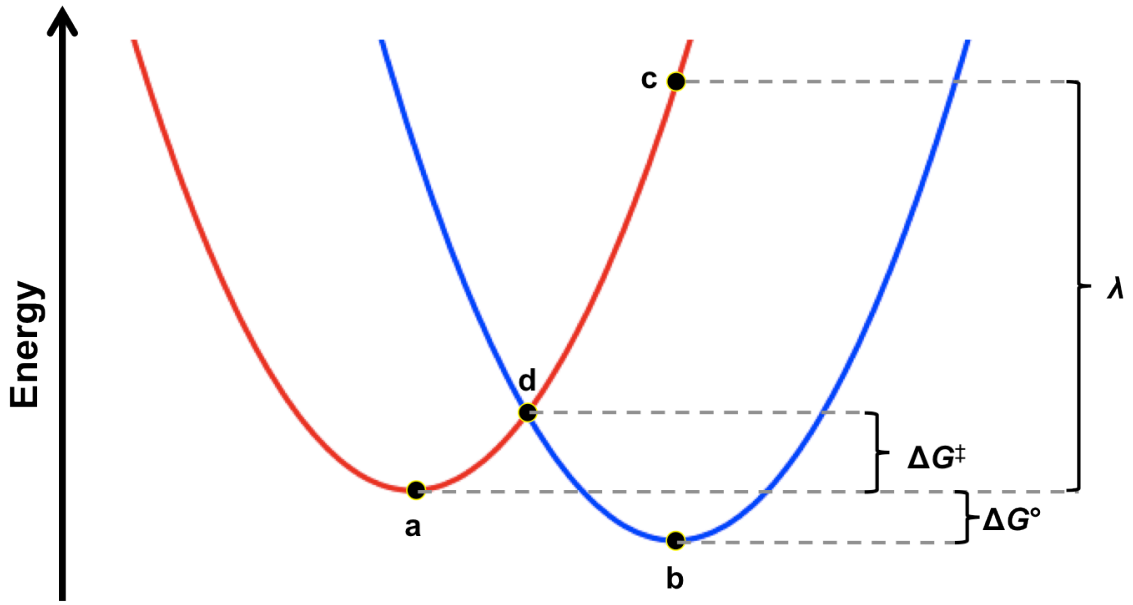

Figure 4.5. Energy diagram illustrating thermodynamic parameters for an ET reaction. The vertical axis is increasing energy; the horizontal axis describes the nuclear coordinate. Reactant state (D•|A): red; product state (D|A•): blue.

The thermodynamic driving force for the reaction ($-\Delta G°$) is given by the difference in energy between the minima of the reactant and product state surfaces (points a and b, respectively). Different nuclear and solvent configurations stabilize the reactant and product states (the energy minima are at different positions along the horizontal axis); thus, both inner sphere (nuclear) and outer sphere (solvent) rearrangements must accompany the ET reaction. This reorganization energy, λ, is a sum of nuclear (λ_{inner}) and solvent (λ_{outer})

components. In **Figure 4.5**, λ is defined as the difference in energy of the reactant (or product) state in the reactant (a) and product configurations (c).

The Franck-Condon principle states that the movement of electrons is much faster than the movement of nuclei. For thermal ET to occur with conservation of energy, the reactant and product geometries (and energies) must be equal. This is the point at which the reactant and product state surfaces intersect (d). The energy difference between the reactant state minimum (a) and this intersection (d) is the activation energy ($\Delta G^{\ddagger}$) required in order for the reaction to proceed.

For ET to occur, the two diabatic states must mix to form two adiabatic states (**Figure 4.6**, dashed lines). The electronic coupling matrix element which mixes the reactant and product states is known as H_{AB}; the energy difference at the point of intersection between the upper and lower adiabatic curves is equal to $2H_{AB}$. From this diagram, it should be evident that enhanced electronic communication between the reactant and product states (larger H_{AB}, and more mixing between the states) lowers the activation barrier for thermal ET.

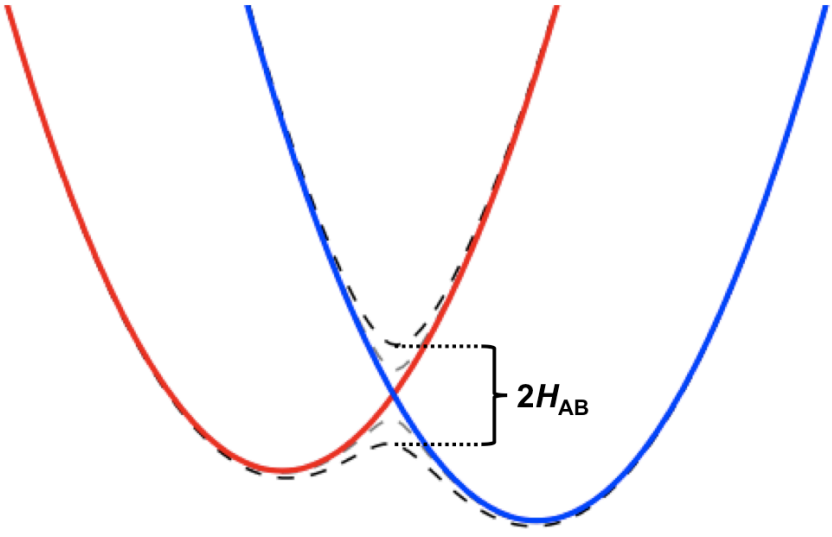

Figure 4.6. Energy diagram illustrating diabatic (solid lines) and adiabatic (dashed lines) states, and the coupling parameter H_{AB}.

The specific rate of ET (k_{ET}) between donor and acceptor can be described by Equations 4.1 and 4.2. (For more details on the origin and development of this equation, the curious reader is directed to papers by R. A. Marcus[15–18]).

$$k_{ET} = \sqrt{\frac{4\pi^3}{h^2 \lambda k_B T}} H_{AB}{}^2 \exp\left(\frac{-(\Delta G^\circ + \lambda)^2}{4\lambda k_B T}\right) \tag{4.1}$$

$$H_{AB} = H_{AB}(r_0)\exp\left(-\frac{1}{2}\beta(r - r_0)\right) \tag{4.2}$$

Here, k_B and h are the Boltzmann and Planck constants, respectively. The ET rate is dependent on reaction driving force ($-\Delta G^\circ$), reorganization energy (λ), and distance between electron/hole donor and acceptor (r). H_{AB} is related to the D-A distance by Equation 4.2, where β is the decay constant for tunneling, r_0 is the limit of contact (taken as the sum of van der Waals radii), and r is as given above. In general, ΔG° and λ depend on D and A molecular composition and local environment, while H_{AB} is a function of D-A distance and the structure of the intervening medium (described by β).

If all other parameters are held constant, increased driving force (more negative ΔG° values) results in increased ET rate – but only up to a point. The maximum ET rate occurs when $-\Delta G^\circ$ is equal to λ; this is known as a "driving force optimized" reaction. Further increases in driving force result in decreased ET rates; this is known as the "inverted region."

For reactions that are driving force optimized, the exponential term in Equation 4.1 becomes unity, and the ET rate depends primarily on donor-acceptor distance and the intervening medium. Assuming that λ is constant across a series, it can be seen from Equation 4.2 that a plot of $\log(k_{ET})$ is linearly proportional to the D-A separation (r-r_0), with a slope that is proportional to β.

Experimental Measurements

Investigations by the Gray group and others have probed this driving force optimized regime in abiological model systems (small molecules, frozen organic glasses) and proteins. By analyzing aggregate data from myriad experiments, a tunneling timetable can be constructed to describe the distance dependence of ET through different media, including proteins (**Figure 4.7**). As described by semiclassical theory, $\log(k_{ET})$ is linearly related to the D-A separation (r-r_0), with a slope that is proportional to β.

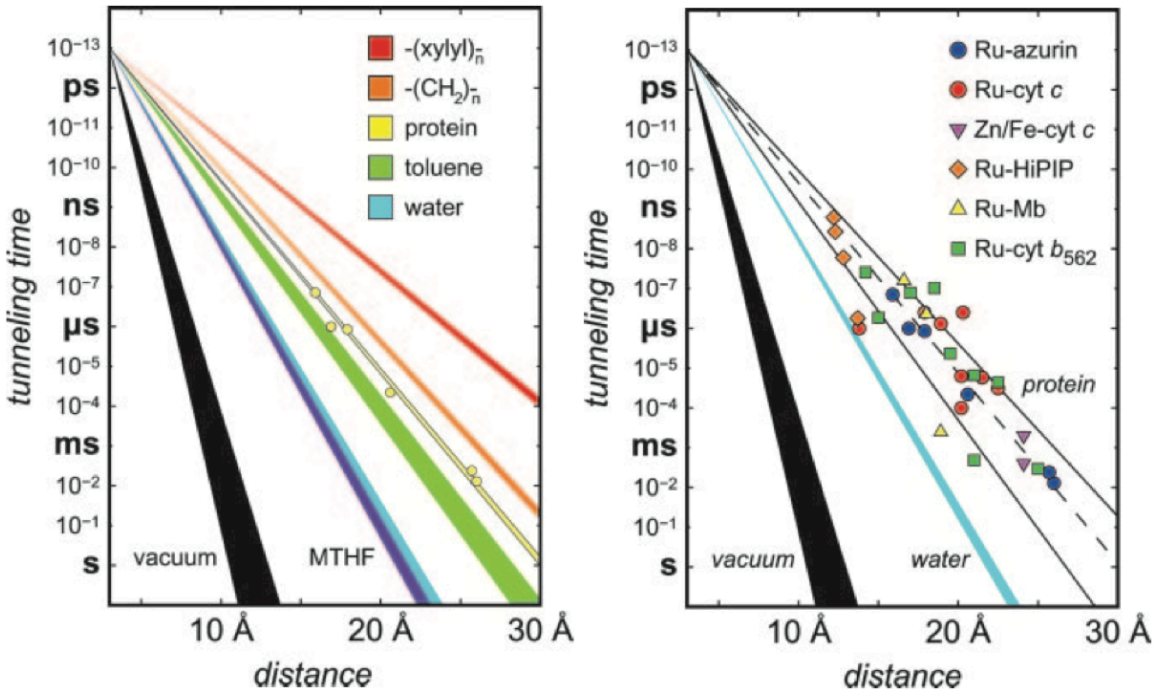

Figure 4.7. Tunneling timetables for driving force-optimized ET reactions.[19] The "tunneling time" on the y-axis is the inverse of the ET rate constant. **Left**: comparison of ET through different media. **Right**: comparison of ET rates for different protein systems.

One of the most important messages in **Figure 4.7** is that as D-A distances increase linearly, the ET time increases exponentially. Single-step ET processes over large distances (> 30 Å, such as the width of a membrane bilayer), could take

minutes or days, even for reactions that are driving force optimized. Another mechanism is needed to accomplish such long-distance ET events rapidly enough to support cellular processes. As will be demonstrated, breaking the overall ET event into multiple shorter (and therefore faster) hopping steps can allow the net ET reaction to proceed on a relevant timescale.

4.3. Multistep electron transfer

If there is an additional redox site between D and A that can accommodate an electron/hole, the overall transfer from D to A can occur in two shorter-distance (and potentially faster) tunneling steps; D to I, then I to A. In order to understand natural and model biological systems, and other multistep ET reactions, we would like to compare these hopping pathways to those of single-step ET. Since each of the hopping steps obeys the ET rate dependence based on its individual values of ΔG°, λ, and r, we can calculate the overall hopping reaction rate and compare it to that for single-step tunneling, to see if there is a "hopping advantage."

Two-step hopping requires three sites: the initial electron (hole) donor (D), a relay station to which this electron (hole) is temporarily transferred (I), and the final electron (hole) acceptor (A). Oxidized or reduced I is a real intermediate that, in principle, can be detected spectroscopically. It is helpful to think of these three sites together as a single system that can be described by the location of the electron/hole, as shown in Equations 4.3a-c.

$$X = D^{+/-} \cdots I \cdots A \tag{4.3a}$$

$$Y = D \cdots I^{+/-} \cdots A \tag{4.3b}$$

$$Z = D \cdots I \cdots A^{+/-} \tag{4.3c}$$

We write the hopping reactions as follows:

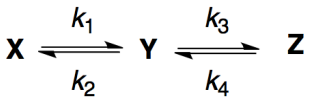

The corresponding rate equations are given in Equations 4.4a-c:

$$\frac{d[X]}{dt} = -k_1[X] + k_2[Y] \tag{4.4a}$$

$$\frac{d[Y]}{dt} = k_1[X] - k_2[Y] - k_3[Y] + k_4[Z] \tag{4.4b}$$

$$\frac{d[Z]}{dt} = k_3[Y] - k_4[Z] \tag{4.4c}$$

By solving this set of differential equations, we obtain expressions for each of the concentrations as functions with respect to time (i.e., $[X](t)$, $[Y](t)$, $[Z](t)$). We assume that the initial concentrations of Y and Z are zero; the resulting equations are more complicated without this assumption. Mathematica software (Wolfram Research) can be used to solve these equations analytically. We are interested in the overall electron transfer rate constant from the initial donor to the acceptor, therefore, the function $[Z](t)$ is particularly useful. The very lengthy output from Mathematica for $[Z](t)$ can be simplified to the following form (Equation 4.5):

$$[Z](t)_{hopping} = \frac{[X]_0 k_1 k_3}{2bc}\left[2c - \left(c - a\sqrt{c}\right)\exp\left(\frac{1}{2}\left(-a - \sqrt{c}\right)t\right) - \left(c + a\sqrt{c}\right)\exp\left(\frac{1}{2}\left(-a + \sqrt{c}\right)t\right)\right] \tag{4.5}$$

where a, b, and c are defined as:

$$a = k_1 + k_2 + k_3 + k_4 \tag{4.6a}$$

$$b = k_1k_3 + k_1k_4 + k_2k_4 \tag{4.6b}$$

$$c = a^2 - 4b \tag{4.6c}$$

Eventually we will want to compare the overall rates of single-step ET and two-step hopping, therefore, an analogous expression for $[Z](t)$ using the single-step mechanism must be defined.

$$\mathbf{X} \underset{k_6}{\overset{k_5}{\rightleftharpoons}} \mathbf{Z}$$

$$X = D^{+/-} \cdots A \tag{4.7a}$$

$$Z = D \cdots A^{+/-} \tag{4.7b}$$

Solving the differential equations in the same manner as described above, the single-step expression is given in Equation 4.8, again assuming that $[Z]_0$ is 0.

$$[Z](t)_{tunneling} = \frac{[X]_0 k_5 \left[1 - \exp\left(-\left(k_5 + k_6\right)t\right)\right]}{k_5 + k_6} \tag{4.8}$$

Comparison of the $[Z](t)$ functions for both mechanisms (Equations 4.5 and 4.8, respectively) shows that hopping is a biexponential process, while single-step tunneling is monoexponential. In order to compare these two mechanisms directly (and determine the rate advantage for hopping), we need to determine an average ET time (τ). The "survival probability" function, $F(t)$ (Equation 4.9) gives the probability (from zero to one) that an electron at any point in time will have *not yet* undergone the complete ET to generate product (Z).

$$F(t) = \frac{[Z](t) - [Z](\infty)}{[Z](0) - [Z](\infty)} \tag{4.9}$$

Integration of this function ($F(t)$) gives the desired average ET time (Equation 4.10).

$$\tau = \int_0^\infty F(t)dt \tag{4.10}$$

Substitution with the $[Z](t)_{\text{hopping}}$ and $[Z](t)_{\text{tunneling}}$ functions from Equations 4.5 and 4.8 gives:

$$\tau_{hopping} = \frac{k_1 + k_2 + k_3 + k_4}{k_1k_3 + k_1k_4 + k_2k_4} \tag{4.11}$$

$$\tau_{tunneling} = \frac{1}{k_5 + k_6} \tag{4.12}$$

For construction of the hopping map, we are interested in average ET time with respect to $\Delta G°$ of the first hopping step, which is the branching point between the two mechanisms, as well as the driving force of the overall reaction. Accordingly, the expressions for τ in terms of rate constants (k_1 through k_6) must now be converted to expressions in terms of $\Delta G°$ and the other ET parameters (β, λ, H_{AB}, r). Substitution of Equation 4.2 into Equation 4.1 and collection of constants yield a general equation for a single-step tunneling:

$$k_{ET} = C_0 \exp\left(-\beta\left(r - r_0\right) - \frac{\left(\Delta G° + \lambda\right)^2}{4\lambda k_B T}\right) \tag{4.13}$$

$$C_0 = \sqrt{\frac{4\pi^3}{h^2\lambda k_B T}}\left(H_{AB}(r_0)\right)^2 \tag{4.14}$$

We also define expressions for the reverse rate constants (k_2, k_4) in terms of forward rate constants (k_1, k_3) by using the definition of $\Delta G°$:

$$k_2 = k_1 \exp\left(\frac{\Delta G^\circ_{DI}}{k_B T}\right) \tag{4.15}$$

$$k_4 = k_3 \exp\left(\frac{\Delta G^\circ_{IA}}{k_B T}\right) \tag{4.16}$$

$$\Delta G^\circ_{DA} = \Delta G^\circ_{DI} + \Delta G^\circ_{IA} \tag{4.17}$$

where $\Delta G^\circ_{\mathrm{DI}}$ and $\Delta G^\circ_{\mathrm{IA}}$ are the standard free energy changes for the first and second hopping steps, respectively, and $\Delta G^\circ_{\mathrm{DA}}$ is the overall reaction free energy change. Note that this notation assumes that the reaction starts from a donor, D. Depending on the particular system, this can be either an electron donor or a hole donor. Substitution of Equations 4.13-4.16 into Equations 4.11 and 4.12 and subsequent simplification yields τ in terms of the ET parameters (Equations 4.18 and 4.19). These expressions have been simplified by assuming that a single β and λ apply for all ET reactions in the system, but this is not necessary (as will be seen for hopping maps, vide infra).

$$\tau_{hop} = \frac{\exp\left(\beta\left(r_2 - r_0\right) + \frac{\left(\Delta G^\circ_{IA} + \lambda\right)^2}{4\lambda RT}\right)\left(1 + \exp\left(\frac{\Delta G^\circ_{DI}}{RT}\right)\right) + \exp\left(\beta\left(r_1 - r_0\right) + \frac{\left(\Delta G^\circ_{DI} + \lambda\right)^2}{4\lambda RT}\right)\left(1 + \exp\left(\frac{\Delta G^\circ_{IA}}{RT}\right)\right)}{C_0\left(1 + \exp\left(\frac{\Delta G^\circ_{IA}}{RT}\right) + \exp\left(\frac{\Delta G^\circ_{DA}}{RT}\right)\right)} \tag{4.18}$$

$$\tau_{tunneling} = \frac{1}{C_0 \exp\left(-\beta\left(r_T - r_0\right)\right)\left(\exp\left(\frac{-\left(\Delta G^\circ_{DA} + \lambda\right)^2}{4\lambda RT}\right) + \exp\left(\frac{-\left(\Delta G^\circ_{DA} - \lambda\right)^2}{4\lambda RT}\right)\right)} \tag{4.19}$$

The values r_1, r_2, and r_{T} correspond to the D–I, I–A, and D–A distances, respectively. Note that these are straight-line distances, so r_{T} need not be the sum of r_1 and r_2.

Substitution of Equation 4.18, using Equation 4.17, gives $\tau_{hopping}$ in terms of $\Delta G°_{DI}$ and $\Delta G°_{DA}$. The dependence of $\tau_{hopping}$ on $\Delta G°_{DA}$ and $\Delta G°_{IA}$ can be represented graphically on a hopping map. The values of $\tau_{hopping}$ span many orders of magnitude, so we construct contour plots of $-\log_{10}(\tau_{hopping})$ (represented by the color gradient), with $-\Delta G°_{DA}$ as the x-axis, and $-\Delta G°_{DI}$ as the y-axis.

A computer program for the construction of hopping maps is available for download at http://www.bilrc.caltech.edu. The Matlab scripts used to generate this program also can be found in Appendix D.

4.4. Construction of Hopping Maps: an example for Re-Azurin

We will first examine use of the hopping map program to construct a hopping map for a known rhenium-labeled azurin system in which tryptophan acts as the redox intermediate.[20]

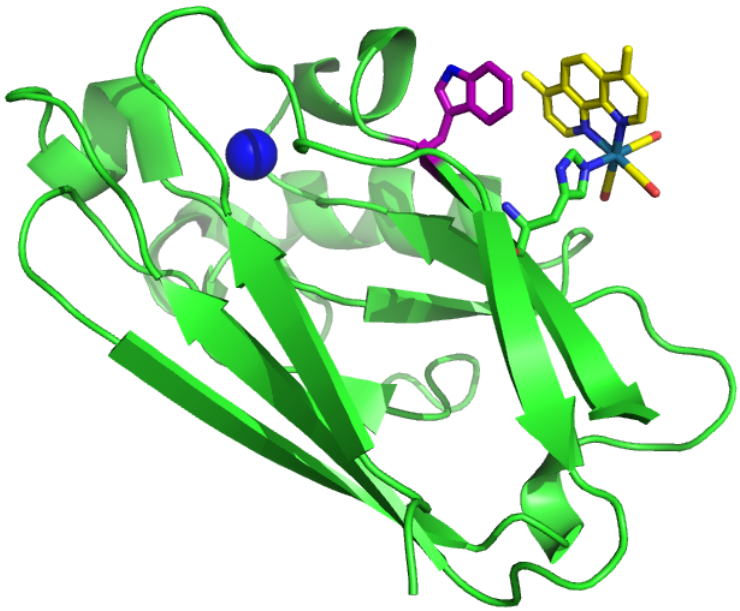

Figure 4.8. The Re_{H124}-W_{122}-Azurin hopping system. The Re photosensitizer is highlighted in yellow, W122 in purple, and the Cu center in blue. PDB 2I70.

Inputs in two prompts are required to generate each map. The first prompt requests the ET parameters for the system of interest, namely temperature T (K), donor-intermediate-acceptor distances r (Å), and the parameters β (Å^{-1}), and λ (eV) (**Figure 4.9**).

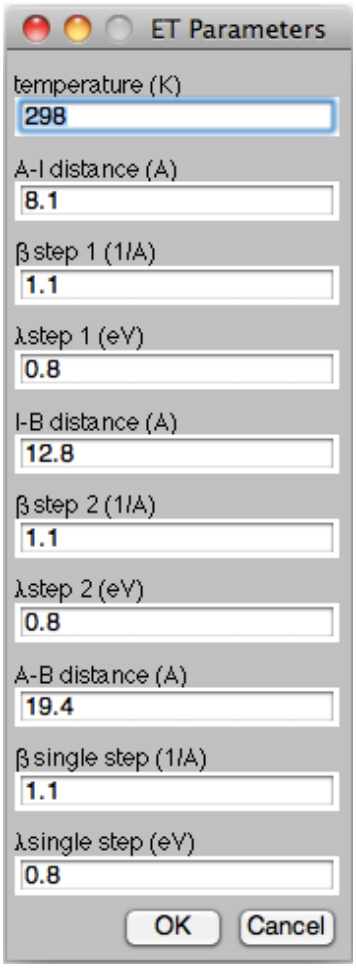

Figure 4.9. Prompt #1: ET parameters. In this notation, "A" is the donor, or starting point, "I" is the intermediate, and "B" is the acceptor, or end point of the ET reaction.

In all cases, the van der Waals contact (r_0) is assumed to be 3 Å, and $H_{AB}(r_0)$ is 0.0231 eV. These parameters affect the rates and contours associated with each map. For demonstration purposes, the default variables in this prompt are those used for the Re_{H124}-W_{122}-Azurin system. Note that the hopping map program

allows variation of β and λ values for each individual ET. For all analyses in this Chapter, we will use constant β and λ values within a system. The effect of variability/uncertainty in each ET parameter is discussed in Section **4.5**.

Pressing "OK" in the first prompt brings up a second one (**Figure 4.10**). This prompt accepts parameters that define hopping map visualization: the range of driving forces to be examined ($\Delta G_{DI}°$ and $\Delta G_{DA}°$, eV), resolution, and contour intervals. Note that these parameters do not affect the fundamental hopping rates associated with a given system. Maps with larger range and higher resolution take more time to generate; this prompt gives the user control over the speed and quality with which each map is generated.

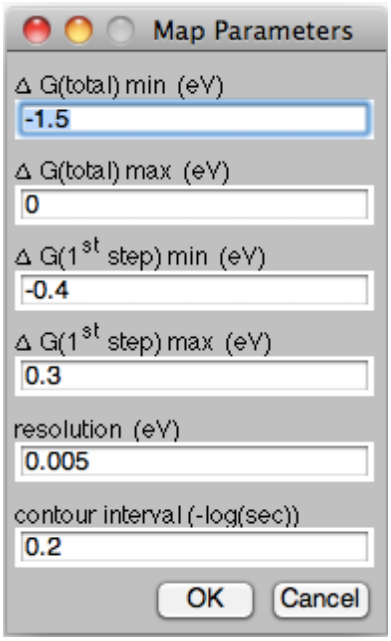

Figure 4.10. Prompt #2: Hopping Map parameters

Pressing "OK" in the second prompt will generate the hopping map. Once the map has been generated, the prompts will re-appear, to allow construction of another map. This time, the default parameters are the previously input values. When no more maps are desired, pressing "Cancel" on both prompts exits the program.

A sample hopping map for Re_{H124}-W_{122}-Azurin has been generated using the values shown above **Figure 4.11**. The program output includes the hopping map with labeled axes, a record of the ET parameters used in the generation of this map, and a color bar indicating the hopping time associated with each color.

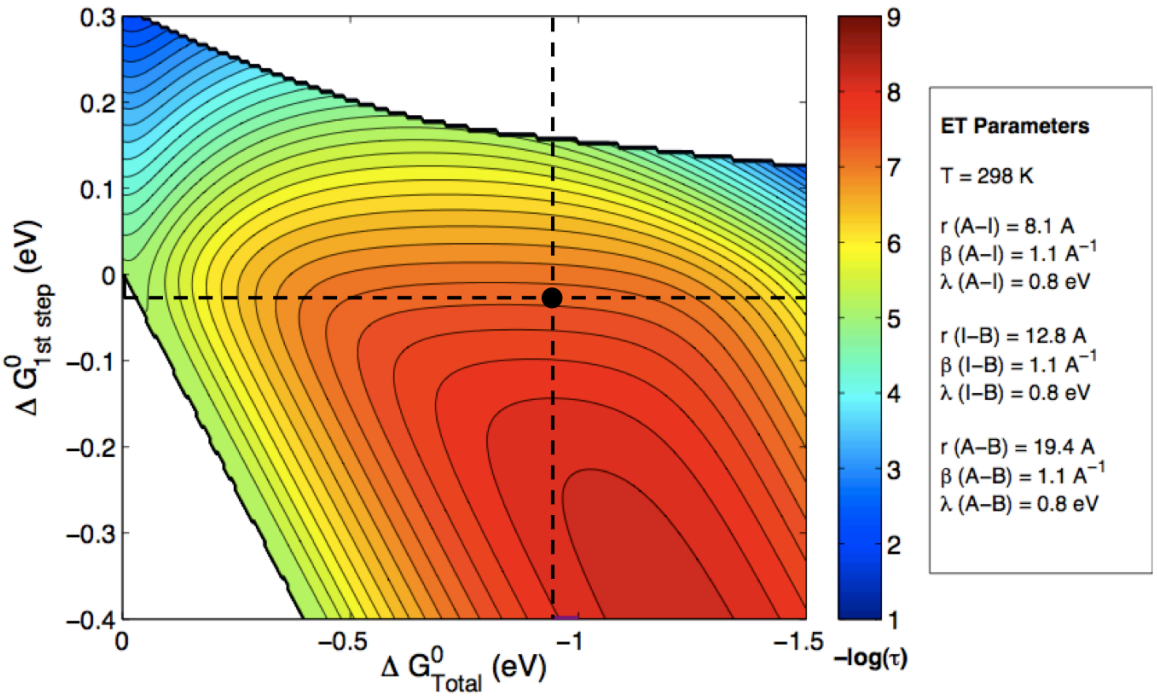

Figure 4.11. Sample hopping map for Re_{H124}-W_{122}-Azurin. ET parameters are displayed in the side bar. A black dot has been placed at $\Delta G_{total}° = -0.94$ eV, $\Delta G_{1st\ step}° = -0.028$ eV.

The color contours represent the predicted hopping time, for any given $\Delta G_{DI}°$ for intermediate formation, and $\Delta G_{DA}°$ for the complete reaction. Redder, or "hotter" regions indicate faster hopping and smaller time constants τ. For example, the reddest, most inner region of this map ($\Delta G_{DI}° \sim -0.3$ eV, $\Delta G_{DA}° \sim -1.2$ eV) corresponds to a $-\log(\tau)$ value of 8.2-8.3, or a hopping time of 5-6 ns; the bluest edge (upper left corner) corresponds to a $-\log(\tau)$ value of 2.2-2.4, or a hopping time of 4-6 ms.

Two portions of the map are shown in white; these are regions in which we would not predict to observe hopping. The region in the upper right is one in which $\tau_{hopping}/\tau_{tunneling} < 1$; in other words, where hopping is predicted to be equal to or slower than single-step ET. As will be seen, the position and shape of this perimeter vary based on the assumed ET parameters. The bottom left hand corner, to the left of the solid black line, is the region in which the second hopping step is endergonic. In this case, the intermediate acts as an electron/hole sink, instead of promoting the second ET step. This black line corresponds to $\Delta G_{DI}° = \Delta G_{DA}°$, and is the same for all maps.

By examining the driving forces at work in Re_{H124}-W_{122}-Azurin, we can place this system on the map and compare predicted and experimental ET rates. The driving force for the first ET step (tryptophan oxidation) was determined to be –28 meV, based on kinetics analysis of the forward and reverse ETs between W122 and *Re.[20,21] On the map, this regime is indicated by a horizontal dashed line. Photo-induced metal-to-ligand charge transfer (MLCT) generates a highly oxidizing triplet excited state ($^*Re^{II}dmp^{\bullet-}$); this excited state potential ($E°(^*Re^{II}dmp^{\bullet-}/(Re^{I}dmp^{\bullet-}))$ is taken to be 1.25 V vs. NHE; all reduction potentials are vs. NHE, unless otherwise noted.[22,23] The azurin $Cu^{II/I}$ potential was determined at 0.31 V (pH 7).[24] Thus, the overall driving force is 0.94 eV. The black dot in **Figure 4.11** represents this location, with a predicted time constant of 44 ns. This within a factor of 2 of the experimentally determined time constant (31 ns).[20]

A number of important features are evident in the hopping map. In cases where the first hop occurs with little driving force ($\Delta G_{DI}° \sim 0$, on the vertical axis), the horizontal nature of the map contours indicates that overall ET rate is much more sensitive to changes tryptophan oxidation ($\Delta G_{DI}°$) than in the overall driving force ($\Delta G_{DA}°$). As an example, let's again examine the black dot on the map. Increasing

or decreasing the driving force for tryptophan oxidation by 50 mV (without affecting the overall driving force) results in a range of time constants of 54-570 ns, variation by an order of magnitude. Similar variation in total driving force (without affecting the driving force for tryptophan oxidation) only results in a range of 145-160 ns, roughly 10% variability. Conversely, for systems in which $\Delta G_{DI}°$ is very negative (bottom rows of the map), the contours are more vertical, and total ET time (τ) is much more dependent on the overall driving force.

Another key feature is the border along the upper right hand corner. This indicates that the multistep advantage is lost for systems in which the first ET event is endergonic by more than ~200 mV. Such systems may still undergo ET, but it is more likely to proceed via single step tunneling.

A final observation is that the hopping map displays the inverted region with respect to overall driving force; ET times associated with $\Delta G_{DA}° = -1.5$ V are slower than those at $\Delta G_{DA}° = -1.2$ V across the entire range of $\Delta G_{DI}°$.

4.5. ET parameters: selection process, effects, and limitations

For the Re_{H124}-W_{122}-Azurin system, many of the ET parameters can be measured directly, and all of the fundamental rate constants have been determined experimentally by transient luminescence and absorption spectroscopies.[20] However, the values of β, λ, r_1 and r_3 are still subject to interpretation, even for this well-characterized protein system. Additionally, there is debate over the precise reduction potentials (and therefore, driving forces) associated with donor, intermediate, and acceptor. For more complex biochemical systems, the process of selecting parameters and analyzing the hopping map becomes even more complicated.

In this section we use the Re-Azurin system to illustrate the effect that these ET parameters (and uncertainty in their values) have on the rates and shapes associated with the hopping map, and discuss various approaches for determining or estimating these parameters. To facilitate comparison, all hopping maps in this section are scaled to the same ET time (τ) axis: 100 ms (dark blue) to 1 ns (dark red).

Temperature

The first variable requested by the Hopping Map program is temperature. This is often the easiest parameter to determine for an experimental system, and will be ambient temperature (298 K) for a large number of biological systems.

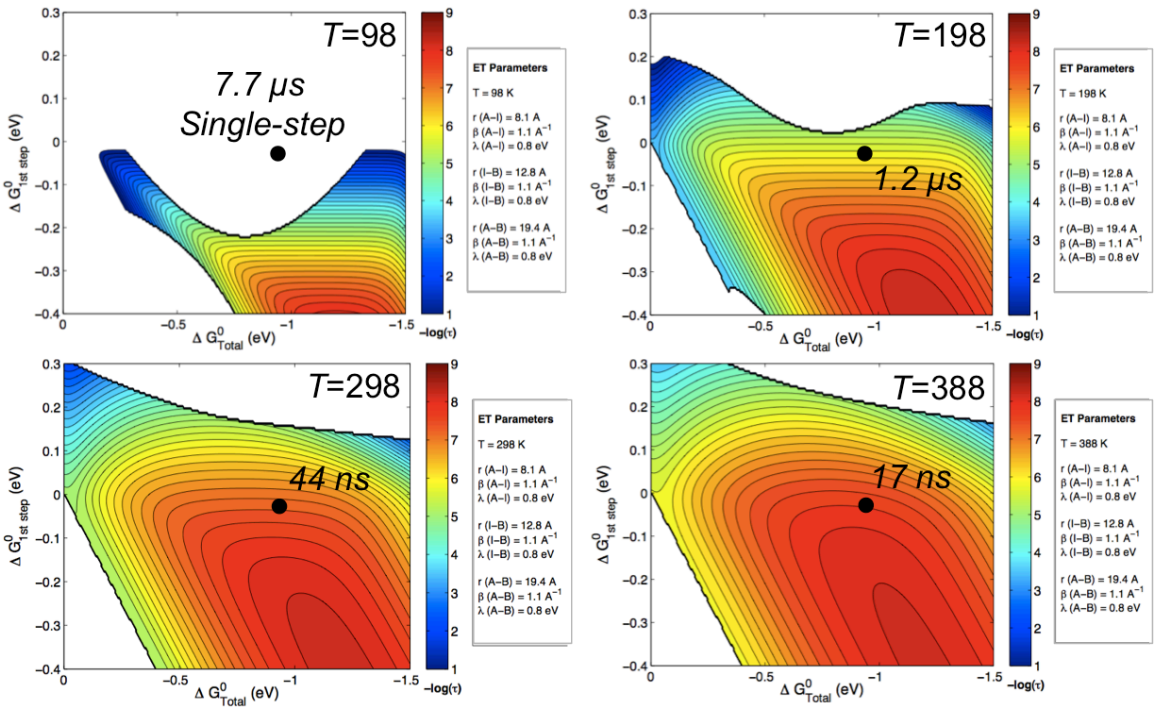

Figure 4.12. Temperature dependence of the Re_{H124}-W_{122}-Azurin hopping map. r_1=8.1 Å, r_2=12.8 Å, r_T=19.4 Å; β=1.1 Å^{-1}; λ=0.8 eV. The black dot is located at $\Delta G_{total}° = 0.94$ eV, $\Delta G_{1st\ step}° = -0.028$ eV.

These maps highlight the fact that the region of hopping advantage shrinks at lower temperature. This indicates that for this system, hopping is more sensitive to temperature than single-step tunneling; it slows down more at low temperatures, and speeds up more at high temperatures. By T= 98 K, we do not expect to observe hopping for Re_{H124}-W_{122}-Azurin.

Another observation from these maps is that the optimal total driving force ($\Delta G_{DA}° = -1.2$ V) is constant across a nearly 300 K range of temperatures. In other words (and, as is expected from Equation 4.1), the inverted region does not shift with temperature. As will be seen, the only parameter that affects the point of inversion is λ.

Distance

In a case such as Re-Azurin, where the ET system has been crystallographically characterized, it seems straightforward to determine values for *r*. However, these straight line distances do not account for specific ET pathways.[25–27] As a first approximation, the total ET distance (Cu to Re) is measured as the straight line between the metal centers: 19.4 Å. However, the intermediate ET steps which transiently oxidize W122 in are not as well defined.

The original, published hopping analysis used distances to and from the tryptophan C2 carbon: (r_1=8.9 Å, r_2=11.1 Å, r_T=19.4 Å).[20] However, for a delocalized, aromatic π system, the electron does not necessarily originate from a single atom. One could, alternatively, use the average distance between the 9 atoms in the Trp indole and the Re or Cu center (r_1=8.1 Å, r_2=12.8 Å, r_T=19.4 Å); these are the distances we have used in the example hopping maps thus far. One could also use the closest edge-to-edge distances (r_1=6.3 Å, r_2=10.8 Å, r_T=19.4 Å). As yet another alternative, one could take into account calculated descriptions of the

highest occupied molecular orbital (HOMO) of indole as the source of the electron for the first ET step, and calculated and experimental formulations of the spin density on Trp radical cation as the source of the hole for the second step.[28] As a simplification of this formulation, we use the average distance of the six benzyl atoms to Re as r_1 (7.4 Å), the average distance of the five pyrrole atoms to Cu as r_2 (11.8 Å) and the Re-Cu distance as r_T (19.4 Å).

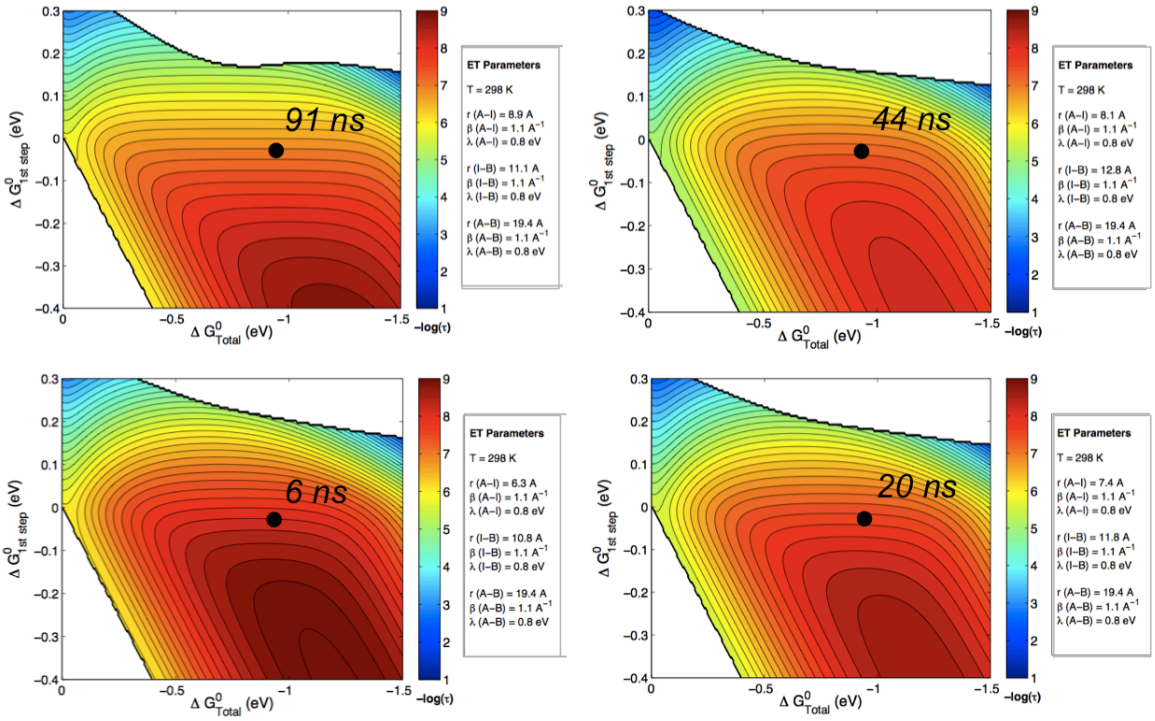

Figure 4.13. Hopping maps for Re_{H124}-W_{122}-Azurin with differing distance formulations. β=1.1 Å^{-1}; λ=0.8 eV. The black dot is located at $\Delta G_{total}°$ = –0.94 eV, $\Delta G_{1st\ step}°$ = –0.028 eV.

These different distance formulations change the rate by just over an order of magnitude (at the black dot), but do not greatly affect the perimeter (area of hopping advantage) or map contours, particularly in the region of interest. We conclude that changes of less than ± 1 Å usually affect the hopping times by less than a factor of 10.

Tunneling decay constant, β

Based on experimental data, the average tunneling decay constant (β) for proteins is 1.1 Å^{-1} (shown in the tunneling timetable (**Figure 4.7**). The original hopping analysis used this value. However, there is significant scatter in the tunneling timetable, and different protein systems may have different decay constants. A superexchange coupling model that takes into account structural complexity can be used to explain this scatter.[26,27,29–33] Experimental determination of β for each individual system is impractical, and so approximations must be made. Knowledge of specific ET pathways facilitates estimation of β. The hopping maps allow us to easily investigate how variation in β results in discrepancies in $\tau_{hopping}$.

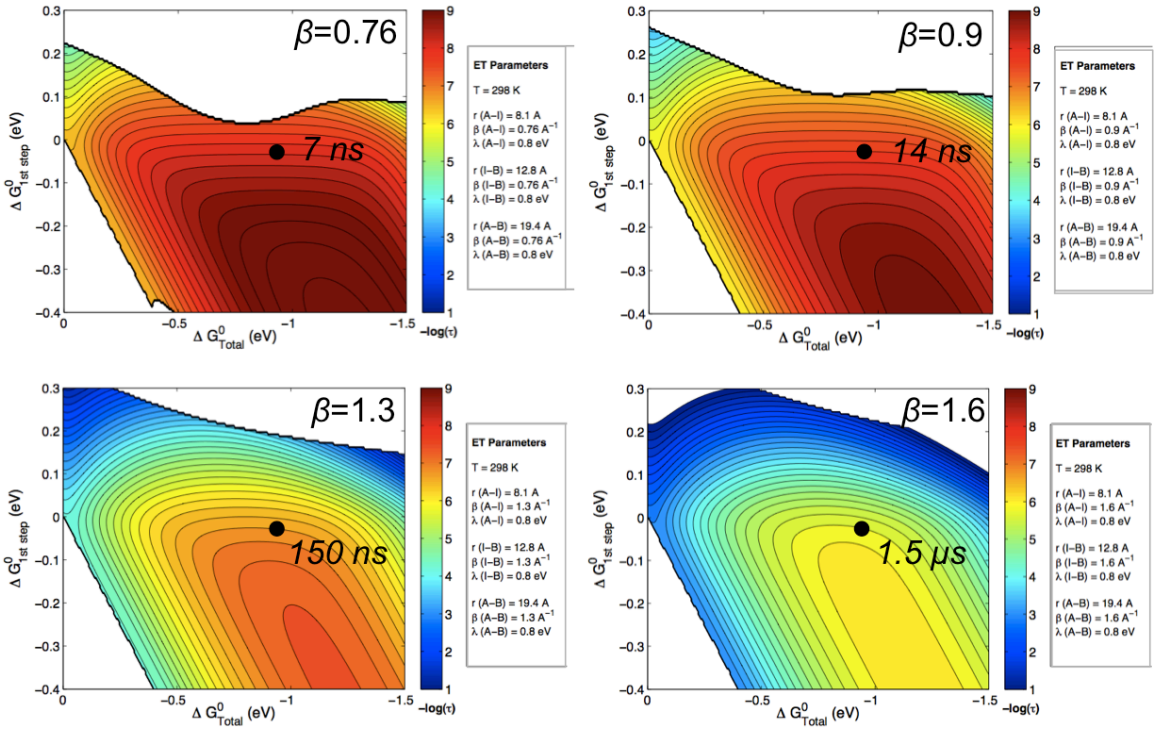

Figure 4.14. Hopping maps for Re_{H124}-W_{122}-Azurin with differing values of β. λ=0.8 eV, r_1=8.1 Å, r_2=12.8 Å, r_T=19.4 Å. The black dot is at $\Delta G_{total}°$ = –0.94 eV, $\Delta G_{1st\ step}°$ = –0.028 eV.

Larger values of β result in increased hopping total ET times, just as in single-step tunneling. In this case, single-step tunneling is more sensitive to β than is hopping; as β (and ET times) decrease, the region of hopping advantage also shrinks. This is opposite what was observed for temperature, where a decrease in ET times was accompanied by an increase in the region of hopping advantage.

Within the context of a protein, the parameter β is essentially bound by the limiting values of tunneling through aqueous glasses (β = 1.6)[34,35] and conjugated xylyl chain (β = 0.76).[36] In practice, the lower bound can be raised further, to that for an alkane chain (β = 1.0).[37] Of the 32 data points for electron-tunneling through the protein medium, (**Figure 4.7**), only two fall above the line of β = 1.0; hopping has been implicated in both cases. In the case of Re_{H124}-W_{122}-Azurin, variation of β by ± 0.2 $Å^{-1}$ (from the starting value of 1.1 $Å^{-1}$) results in increase or decrease in ET time by less than a factor of four.

Reorganization energy, λ

As discussed previously, the reorganization required for a given reaction is composed of both inner- (nuclear) and outer-sphere (solvent) rearrangements. Electron transfer events are charged, by nature. Thus, a polar environment (such as solvation by water molecules) reorganizes more in response to ET. By sequestering redox cofactors within a hydrophobic protein environment, enzymes reduce reorganization and the energy of activation for ET. The inner-sphere reorganization energy of many metalloproteins also is small, particularly when there is no change in spin state, and/or when the ligand geometry is constrained.[38] Experimental reorganization energies have been determined by varying the driving force for single-step ET (**Table 4.1**). The reorganization energy used in the original hopping was 0.8 eV, based on these types of experimental investigations.[9,19]

However, different systems, particularly those not evolved for rapid ET, may have alternate values of λ.

Table 4.1. Reorganization energies for various proteins. Table is adapted from Ref 38.[13,38–45] a: Ref. 39, b: Ref. 13, c: Ref. 40, d: Ref. 41, e: Ref. 42, f: Ref. 43, g: Ref. 44, h: Ref. 45.

	Protein (method)	λ (eV)
Cytochromes	cytochrome c (calculation)[a]	0.69
	cytochrome b5 (calculation)[a]	1.06
	cytochrome c (Ru-cyt c, experimental)[b]	0.74
	cyt c/cyt b5 (experimental)[c]	0.7
Blue Copper	azurin (Ru/Os-Az, experimental)[d]	0.82
	azurin (Ru-Az, experimental)[e]	0.71
	plastocyanin (Ru-Pc, experimental)[f]	0.7 - 0.75
Iron Sulfur Proteins	high-potential Fe_4S_4 (experimental)[g]	< 1
Bacterial Reaction Centers	BRCs (experimental, theoretical)[h]	0.7

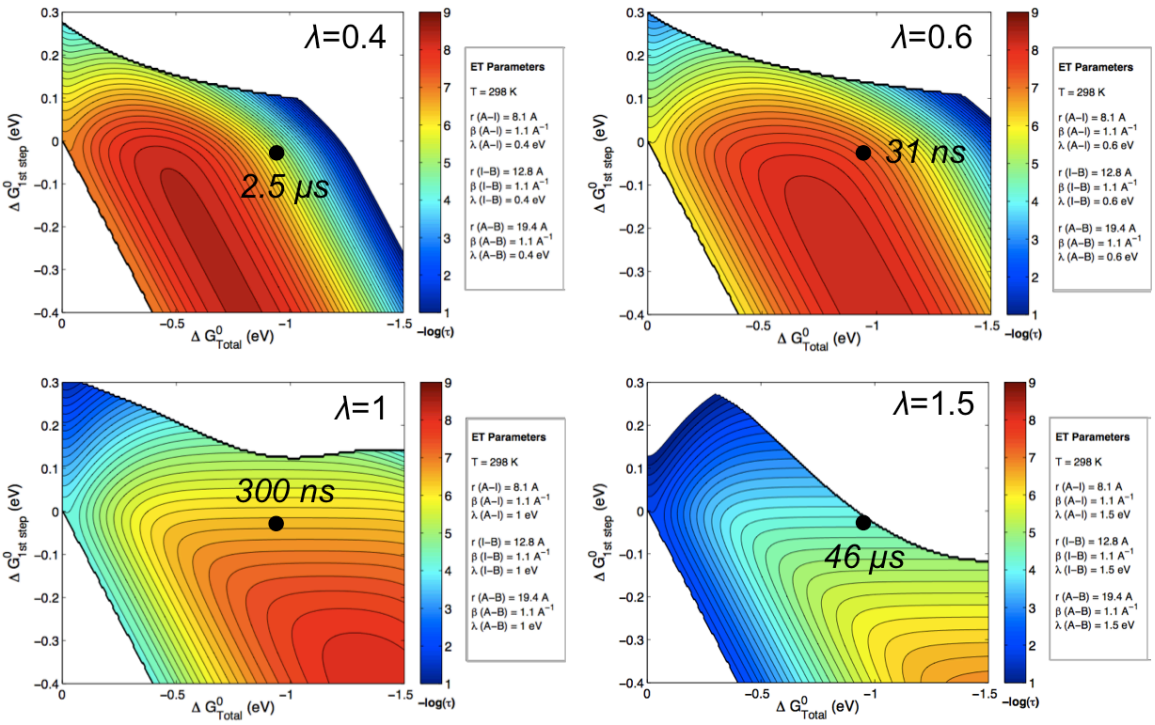

Figure 4.15. Hopping maps for Re_{H124}-W_{122}-Azurin with differing values of λ. β=1.1 Å^{-1}, r_1=8.1 Å, r_2=12.8 Å, r_T=19.4 Å. The black dot is at $\Delta G_{total}°$ = –0.94 eV, $\Delta G_{1st\ step}°$ = –0.028 eV.

Changes in λ affect both the rates and contours of the map. As λ increases, the "hottest" center widens and shifts to more negative values of both $\Delta G_{DA}°$ and $\Delta G_{DI}°$. At the driving forces of interest for the Re_{H124}-W_{122}-Azurin system ($\Delta G_{DA}°$ =–0.94 eV, $\Delta G_{DI}°$=–0.028 eV), there is inversion with respect to λ; the maximum rate occurs at λ=0.6-0.8, and decreases at both smaller and larger values.

Re_{H124}-W_{122}-Azurin is nearly driving force optimized for λ. There is little variation between λ=0.6 and 0.8 eV. However, outside of that optimal range, ET times change dramatically with variation in λ (as is expected). For driving force unoptimized systems in which λ is uncertain, hopping maps provide only a rough approximation of ET times, and must be assessed with care.

Driving forces

The parameters discussed above (T, β, λ, r) are needed for the construction of the map. However, complete hopping analysis requires placing the system of interest on the map, and determining the predicted τ values and rate advantage of hopping. In order to do this, one needs to have knowledge of the driving forces associated with the first and overall ET steps.

Unfortunately, the $E°$ of relevant cofactors often are unknown. Due to the reactivity of many of the intermediates (such as amino acid radicals), there is significant variation in the reported values. Additionally, these potentials can be shifted from the solution values by the protein environment, and, if coupled with protonation/deprotonation, can be affected by pH and hydrogen-bonding.

For example, the solution $W^{+\bullet}$/W potential has been estimated at +1.15 V (water),[22] +1.24 V (water, pH 7),[46] or 0.98 V (water, pH 8).[47] Based on the experimentally measured rate for tryptophan oxidation in Re_{H124}-W_{122}-Azurin

(where W122 is relatively solvent exposed), $\Delta G_{DI}°$ was determined to be –0.028 V; assuming a $^{*}Re^{II}(dmp^{\bullet-})/Re^{I}(dmp^{\bullet-})$ potential of 1.25 V,[22] this places the $W^{\bullet+}/W$ at 1.22 V. Driving forces for ET can be further complicated by changes in protonation state. Tryptophan radical cation is significantly more acidic than the neutral species (pK_a=4.5 vs. ~21).[48] Another redox active amino acid (and potential hopping intermediate), is tyrosine; this intermediate is much more sensitive to pH. The tyrosine neutral species has a pK_a of 10, and a radical cation pK_a of –2.[49] For both of these amino acids, the relevant driving forces are influenced by pH and hydrogen bonding (**Figure 4.16**).

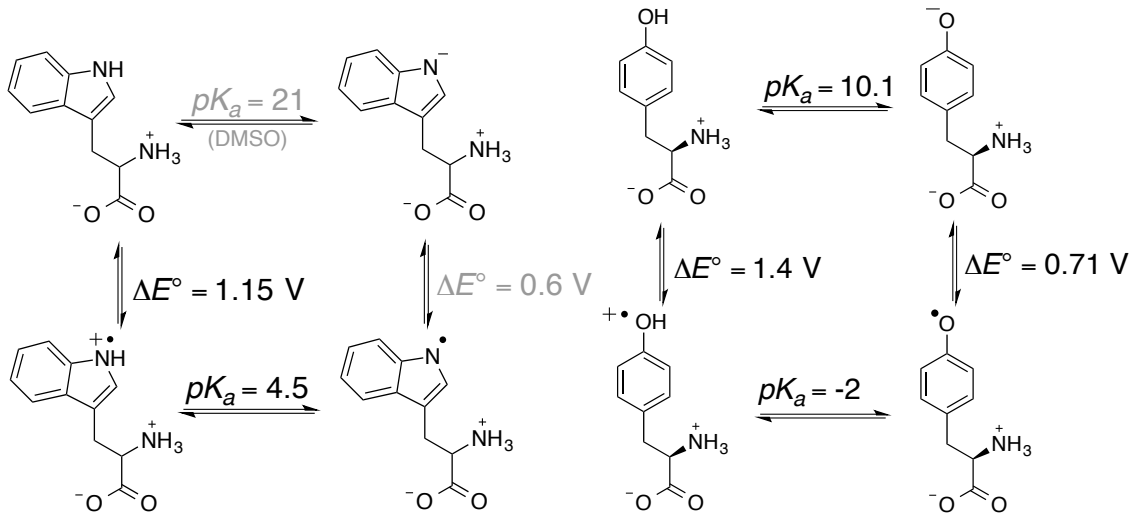

Figure 4.16. Square scheme for tryptophan (left) and tyrosine (right), including relevant reduction potentials and acid dissociation constants.[48,49] Gray values indicate DMSO solutions.

4.6. Hopping Map Limitations

In the best cases, the hopping maps give insight into the advantage of hopping over single-step ET, and provide an estimate of hopping times within an order of magnitude. From the above analysis, small uncertainties in ET parameters (r: ± 1 Å; β ± 0.2 $Å^{-1}$, λ ± 0.1 eV) can change the hopping times (τ) by less than a factor of

10. Additionally, the Hopping Maps program allows quick and facile analysis of the effect of these uncertainties for any given system.

However, these ET parameters can be greatly affected by the specific protein environment, and experimental measurement of many of these parameters is extremely difficult. Even once a hopping map has been constructed with confidence, accurate comparison between computed and experimental hopping rate constants requires accurate assessment of reaction driving forces. This is greatly complicated by the paucity of reliable reduction potential data for biological ET reactions that, for a given cofactor, strongly depend on the protein environment.

Even when exact comparison of experimental and predicted time constants is not possible, assessment of multiple maps can provide a range of expected values, and in some cases, may provide insight into the advantage of hopping over single-step tunneling. We will examine one of these highly underdetermined cases to assess the possibility of hopping in a ruthenium-cytochrome P450 system.

4.7. Application to the P450-W-Ru system

As described previously, we developed a system for phototriggered heme oxidation in a Ru-cytochrome P450 conjugate that requires the presence of a tryptophan situated between Ru and heme sites. We have experimentally determined the rate of porphyrin oxidation, which proceeds on the microsecond timescale with relatively little driving force. By examining a series of hopping maps, we aim to determine the feasibility of oxidative (hole) hopping in this system. Is hopping *possible*? And, based on our analyses, is hopping *probable*?

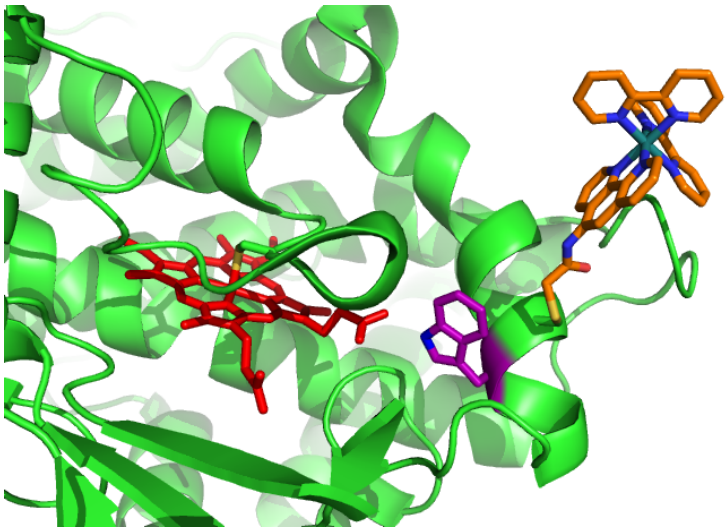

Figure 4.17. Hopping system in Ru_{K97C}-W_{96}-$P450_{BM3}$ (PDB: 3NPL). The P450 heme is highlighted in red, W96 in purple, and the Ru photosensitizer in orange.

Estimates and Challenges

Hopping in the Ru-W-P450 system is underdetermined. Nevertheless, we can make estimates, and probe to what extent error in those estimates affects the hopping map. Temperature is the most certain parameter: 293 ± 2 K. We have no direct measurement of β and λ, but will begin by assuming the typical parameters of β=1.1 $Å^{-1}$; λ=0.8 eV, which apply to many systems (as discussed previously).

The Ru-W-P450 system has been crystallized, and we will use the crystallographic distances as our first estimates for r_1, r_2, and r_T. However, as described for Re_{H124}-W_{122}-Azurin, the ET origin associated with the aromatic tryptophan side chain is ill-defined. Additionally, the hole-acceptor in this case is not a metal center, but the large, conjugated porphyrin ring. Furthermore, the ruthenium photosensitizer is tethered to the protein surface via a flexible acetamido linker. Significant disorder in one unit of the crystal structure, and the biexponential luminescence decay support the existence of multiple conformations (and thus, multiple possible distances) in solution.

The crystallographic Ru-Fe distance is 23.7 Å. We are interested in oxidation of the porphyrin ligand; however, this center is approximately the average of the distances between the photosensitizer and conjugated porphyrin (23.9 Å). We will also examine the distance to the nearest pyrrole edge on the porphyrin: 20.8 Å. It is possible to bring the photosensitizer center even closer to the porphyrin by bending it into a depression in the surface (above the buried heme). Such an arrangement could decrease the through-space Ru-porphyrin distance by as much as 4 Å, and also bring Ru an estimated 2 Å closer to the tryptophan.

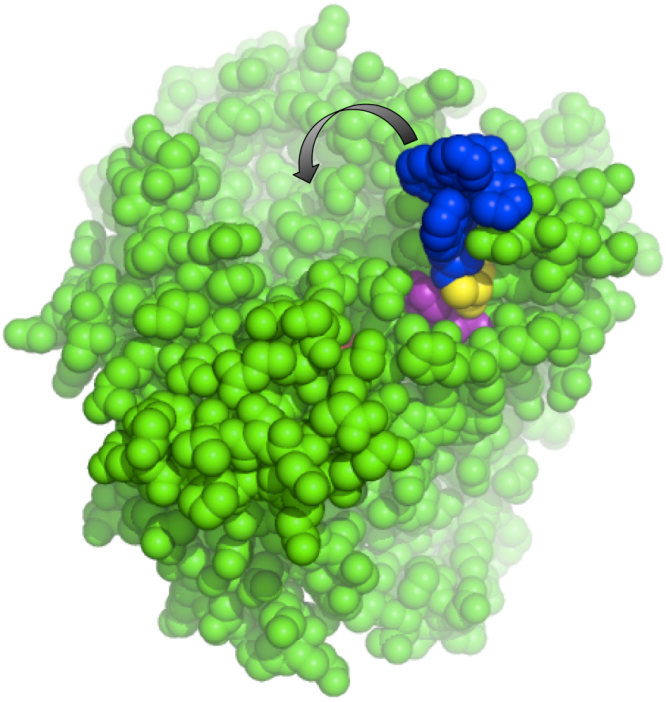

Figure 4.18. Model of the Ru-P450 surface. The photosensitizer is highlighted in blue, the cysteine linker in yellow, W96 in purple, and the buried heme in red.

Finally, we must make estimates for $\Delta G_{total}°$ and $\Delta G_{1st\ step}°$. Instead of placing a dot on the map, we will define a region in which we reasonably expect to find our Ru-P450 system. (As a reminder, all reduction potentials are referenced versus NHE.)

The oxidatively quenched photosensitizer has $E°(Ru^{III/II})$ ≈ 1.3 V.[50,51] The $E°(Fe^{IV/III})$ in other heme enzymes (e.g., horseradish peroxidase) have been reported in a range of 0.72-1 V.[52] A P450 relative, the heme-thiolate enzyme chloroperoxidase, has $E°(Fe^{IV/III})$ estimated at 1.3 V.[53] We will assume that the P450 $E°(Fe^{IV/III})$ is within the range of 0.9-1.3 V, and that the $E°(por^{\bullet+}/por)$ is at or above this value (so that the entire reaction is exergonic). For all analyses, we will use the driving force range: $-\Delta G°_{total}$ = 0 to 0.3 V. As discussed previously, a range of $W^{\bullet+}/W$ potentials have been reported (1-1.3 V), and these can be influenced significantly by hydrogen bonding and protein environment. Therefore, we will assume a range of driving force for first hop step ($-\Delta G°_{1st\ step}$) of –0.10 to +0.3 V.

Single-step tunneling

To provide a comparison for the hopping rates, we will first examine the Ru_{K97C}-W_{96}-$P450_{BM3}$ system using single-step ET (Equations 4.1 and 4.2). Predicted ET times (τ) are listed in **Table 4.2**. Note that at low driving force, with a distance of ~24 Å, single-step ET takes nearly a second.

Table 4.2. Calculated single-step tunneling times for porphyrin oxidation, using a variety of ET parameters.

	r_T (Å)	β (Å^{-1})	λ (eV)	$\Delta G°$(eV)	τ (μs)
Experimental					**1.3**
	23.9	1.1	0.8	0	430,000
	23.9	1.1	0.8	-0.3	20,000
	23.9	0.8	0.5	-0.3	190
	20.8	1.1	0.8	0	77,000
	20.8	1.1	0.8	-0.3	670
	20.8	0.9	0.6	-0.3	3
	17	1.1	0.8	0	1,200
	17	1.1	0.8	-0.3	10
	17	0.9	0.6	-0.3	0.1

Hopping Analysis

By constructing a series of hopping maps, we aim to determine whether or not there is a *clear hopping advantage* within reasonable ET parameters. We will systematically vary ET parameters (r, β, λ) for the Ru-P450 system, and determine the effects on two-step hopping versus single-step tunneling. Each map is constructed with the same range of driving forces and same color scale as the Re-W-azurin system (to facilitate comparisons). The range of *expected* driving forces is bordered by dashed lines. Heme oxidation was observed experimentally, so we assume that $-\Delta G°_{DA} > -\Delta G°_{DI}$; in other words, the system does not fall in the white, bottom left corner of the maps.

Table 4.3. Minimum driving forces necessary to obtain the experimental ET time (within a factor of 3) for each hopping map.

	r_1 (Å)	r_2(Å)	r_T(Å)	β (Å^{-1})	λ (eV)	$\Delta G_{DA}°$(eV)	$\Delta G_{DI}°$(eV)	τ (μs)
Experimental								**1.3**
A	13.8	12.9	23.9	1.1	0.8	-0.300	-0.180	3
B	13.8	9	20.8	1.1	0.8	-0.140	-0.140	3
C	12.1	7.7	20.8	1.1	0.8	-0.025	-0.020	3
D	13.8	9	20.8	1	0.8	-0.075	-0.070	3
E	13.8	9	20.8	1.3	0.8	-0.300	-0.295	3
F	13.8	9	20.8	1.1	0.6	-0.005	0	3
G	13.8	9	20.8	1.1	1	-0.290	-0.285	3
H	12	9	17.0	1	0.8	-0.005	0.045	3
I	12	9	17.0	0.8	1.3	-0.250	-0.245	3

Within the context of each map, we can also determine minimum driving forces to give a time constant within a factor of three of the experimental value; these are given in **Table 4.3**. These values are mainly intended to orient the reader to the map, not to place the Ru-W-P450 system at a defined driving force.

Varying Distances

We first examine the longest distance for ET (**case A**), using the ruthenium center, the porphyrin centroid (average Ru-por distance = 23.9 Å), and the W centroid (average Ru-W, W-por distances). The other ET parameters are β=1.1, λ=0.8, as used previously for the original Re_{H124}-W_{122}-Az system. In case A, hopping is clearly advantageous over the entire expected driving force range. The experimental time constant of 1.3 μs can be reproduced (within a factor of three) assuming reasonable driving forces of 300 meV and 180 meV (for $-\Delta G°_{DA}$ and $-\Delta G°_{DI}$, respectively). This is a rate advantage of *four orders of magnitude* compared to single-step ET.

Next, we set r_T as the distance to the nearest edge of the porphyrin: 20.8 Å (**case B**). The horizontal contours in this map (as well as all the others that follow) shows that hopping is limited entirely by the first step: tryptophan oxidation. The region of hopping advantage decreases. However, hopping still beats single-step tunneling within all of the expected driving forces, and the experimental time can be reproduced with milder overall driving forces (~150 meV).

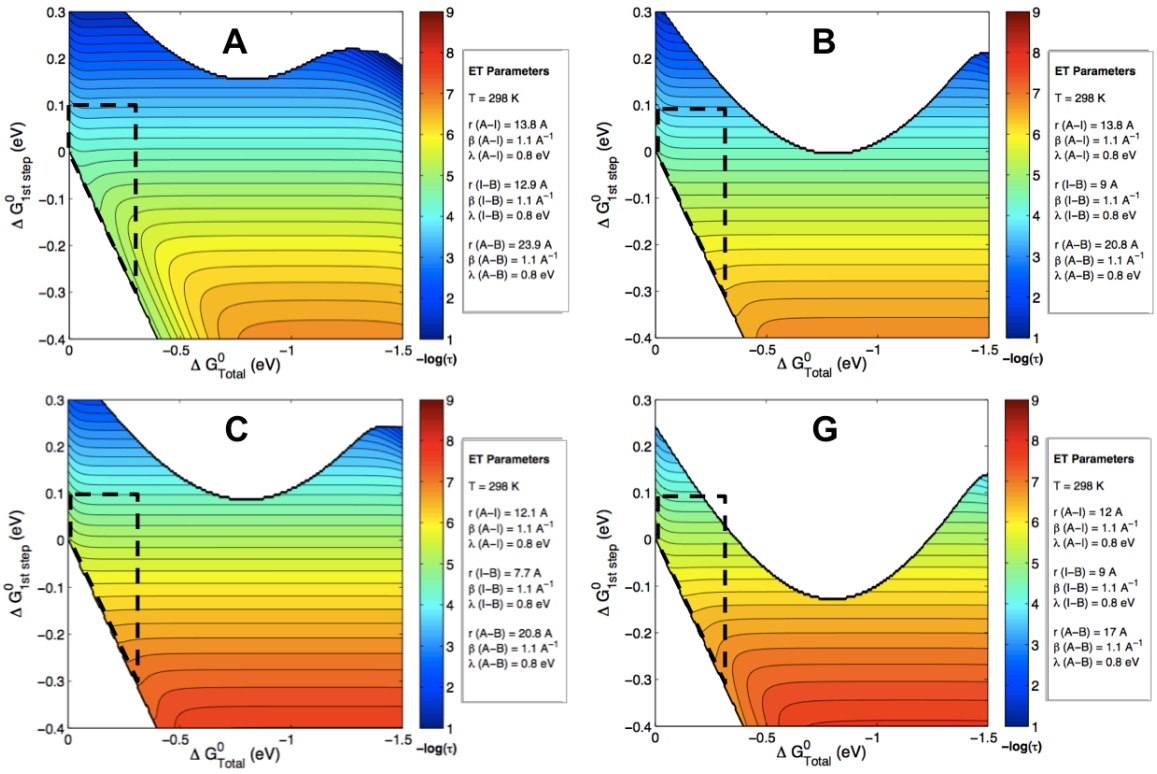

Figure 4.19. Hopping maps for Ru_{C97}-W_{96}-$P450_{BM3}$ heme oxidation: Distance formulations.

If we change the distance formulation to use the tryptophan edges (**case C**) instead of the centroid, we decrease the distance of the first hopping step. This decreases the overall hopping times, and increases the area of hopping advantage. Very little driving force (~ 0.02 eV) is required to reproduce the experimental time constant, using this formulation. Once again, hopping has a rate advantage of four orders of magnitude.

As discussed for the single-step analysis, a final possibility for distances is that the photosensitizer bends over, bringing it in closer proximity to the porphyrin (and also to the tryptophan). Comparison between cases B and G shows that rates increase by over an order of magnitude, and the region of hopping advantage significantly decreases. The hopping advantage is lost only in cases where the first hop is endergonic (>0.05 eV), and the overall driving force is large.

Varying β and λ

We can also examine the effects of uncertainty in β and λ on the Ru_{K97C}-$P450_{BM3}$ hopping map. A significant rate increase is seen by lowering β to 1.0 $Å^{-1}$ (**case D**), and a significant decrease is seen by raising β to 1.3 $Å^{-1}$ (**case E**). However, the region of hopping advantage does not change significantly. Since ET must proceed mainly through bonds, but with at least one through-space hop (between Trp96 and the porphyrin edge), we suspect that the original value of 1.1 $Å^{-1}$ is a reasonable approximation. Changes in λ significantly affect hopping times, and the region of hopping advantage (**cases F and G**). In each case, the experimental time constant can be reproduced, and hopping is advantageous at all expected driving forces.

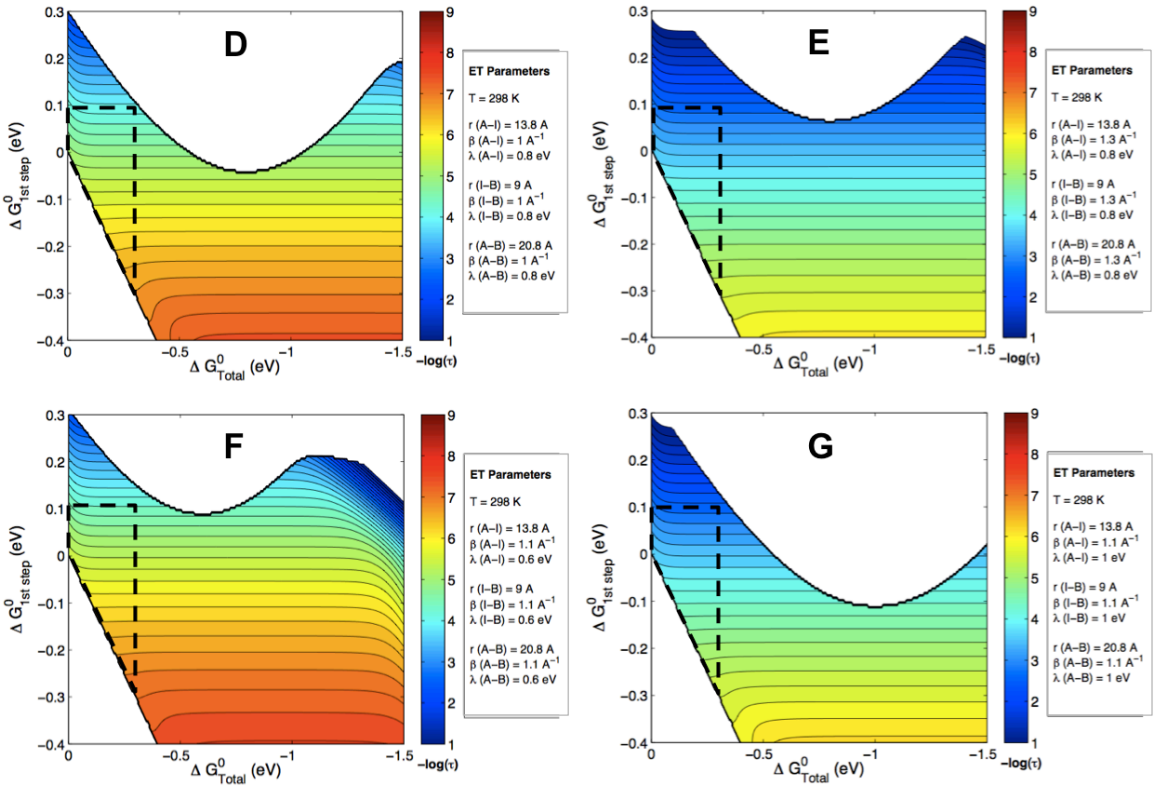

Figure 4.20. Hopping maps for Ru_{K97C}-$P450_{BM3}$ photochemical heme oxidation: Altering β and λ.

All of these maps show a clear hopping advantage, even if single-step ET can reproduce the experimental rate constant within the expected driving forces. What would it take for single-step ET to out-compete hopping?

We present one final, "worst case" hopping scenario (**case I**). r_T is small in comparison to r_1 and r_2 (as the photosensitizer bends toward the P450 surface), β is small (tunneling through a conjugated chain), and λ is large. As shown in **Figure 4.21**, the Ru-W-P450 system is situated exactly where hopping is most advantageous: low overall driving force. Even if the first hop (e.g., tryptophan oxidation) is endergonic by 100 mV, the two-step process can be faster.

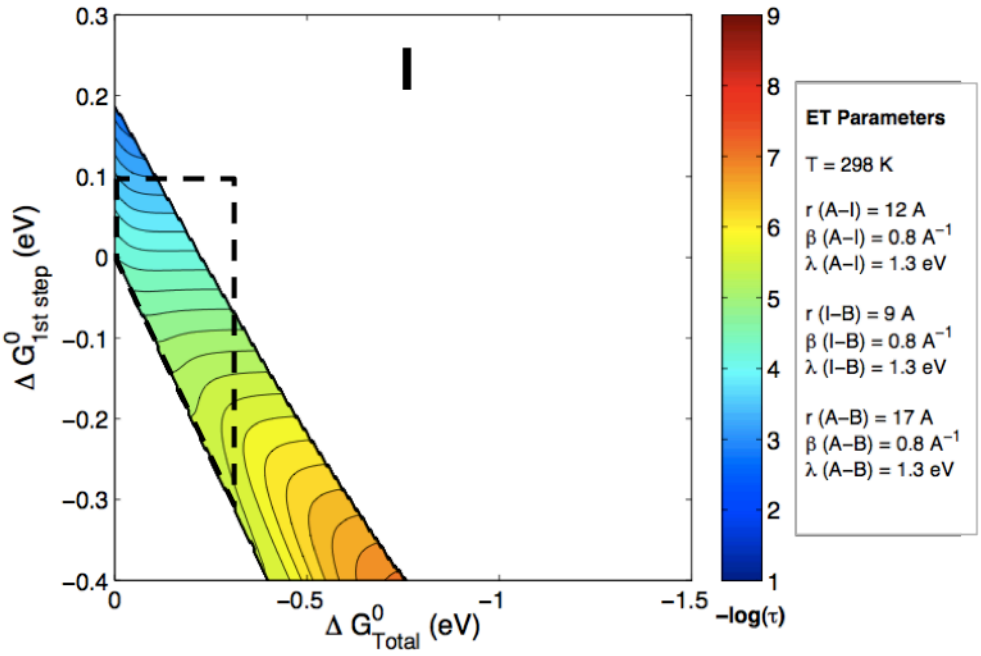

Figure 4.21. Hopping maps for Ru_{K97C}-$P450_{BM3}$ photochemical heme oxidation: Worst case hopping scenario.

These hopping map analyses strongly support the idea of hopping in the Ru-P450 system. In every scenario examined, the experimental rate constant can be easily reproduced with reasonable ET parameters, and there is a rate advantage to hopping in the majority of driving forces.

4.8. Conclusions

This tutorial demonstrates the usage, utility, and limitations of Hopping Maps for the analysis of multistep ET events. We have used this analysis to examine the multistep photochemical heme oxidation in Ru_{K97C}-$P450_{BM3}$, and have shown that there is a clear hopping advantage at nearly all parameters explored. Creation of hopping maps is greatly facilitated by the availability of the hopping map program. However, construction and interpretation of hopping maps that have any relation to real chemical systems requires detailed knowledge of ET parameters.

4.9. Acknowledgments

The original hopping map analysis was conceived of and accomplished by Jay R. Winkler,[20] and his conversations have greatly facilitated construction of this hopping map program. Work for this Chapter was inspired by Harry B. Gray and Jeffrey J. Warren.

4.10. References

(1) Moore, G. F.; Brudvig, G. W. Energy Conversion in Photosynthesis: A Paradigm for Solar Fuel Production. *Annu. Rev. Condens. Matter Phys.* **2011**, *2*, 303–327.

(2) Nelson, N.; Yocum, C. F. Structure and Function of Photosystems I and II. *Annu. Rev. Plant Biol.* **2006**, *57*, 521–565.

(3) Rich, P. R.; Marechal, A. The Mitochondrial Respiratory Chain. *Essays Biochem. Mitochondrial Funct.* **2010**, *47*, 1–23.

(4) Kaila, V. R. I.; Verkhovskky, M. I.; Wikstrom, M. Proton-Coupled Electron Transfer in Cytochrome Oxidase. *Chem. Rev.* **2010**, *110*, 7062–7081.

(5) Lewis, B. A.; Engelman, D. M. Lipid Bilayer Thickness Varies Linearly with Acyl Chain Length in Fluid Phosphatidylcholine Vesicles. *J. Mol. Biol.* **1983**, *166*, 211–217.

(6) Langen, R.; Chang, I.-J.; Germanas, J. P.; Richards, J. H.; Winkler, J. R.; Gray, H. B. Electron-Tunneling in Proteins - Coupling through a Beta-Strand. *Science* **1995**, *268*, 1733–1735.

(7) Regan, J. J.; Di Bilio, A. J.; Langen, R.; Skov, L. K.; Winkler, J. R.; Gray, H. B.; Onuchic, J. N. Electron-Tunneling in Azurin - the Coupling across a Beta-Sheet. *Chem. Biol.* **1995**, *2*, 489–496.

(8) Crane, B. R.; Di Bilio, A. J.; Winkler, J. R.; Gray, H. B. Electron Tunneling in Single Crystals of Pseudomonas Aeruginosa Azurins. *J. Am. Chem. Soc.* **2001**, *123*, 11623–11631.

(9) Gray, H. B.; Winkler, J. R. Electron Tunneling through Proteins. *Q. Rev. Biophys.* **2003**, *36*, 341–372.

(10) Winkler, J. R.; Nocera, D. G.; Yocom, K. M.; Bordignon, E.; Gray, H. B. Electron-Transfer Kinetics of pentaammineruthenium(III)(Histidine-33)-Ferricytochrome-c - Measurement of the Rate of Intramolecular Electron-Transfer between Redox Centes Separated by 15-A in a Protein. *J. Am. Chem. Soc.* **1982**, *104*, 5798–5800.

(11) Casimiro, D.; Richards, J.; Winkler, J.; Gray, H. Electron Transfer in Ruthenium-Modified Cytochromes C. .sigma.-Tunneling Pathways through Aromatic Residues. *J. Phys. Chem.* **1993**, *97*, 13073–13077.

(12) Meade, T. J.; Gray, H. B.; Winkler, J. R. Driving-Force Effects on the Rate of Long-Range Electron Transfer in Ruthenium-Modified Cytochrome c. *J. Am. Chem. Soc.* **1989**, *111*, 4353–4356.

(13) Mines, G. A.; Bjerrum, M. J.; Hill, M. G.; Casimiro, D. R.; Chang, I.-J.; Winkler, J. R.; Gray, H. B. Rates of Heme Oxidation and Reduction in Ru(His33)cytochrome c at Very High Driving Forces. *J. Am. Chem. Soc.* **1996**, *118*, 1961–1965.

(14) Pizano, A. A.; Lutterman, D. A.; Holder, P. G.; Teets, T. S.; Stubbe, J.; Nocera, D. G. Photo-Ribonucleotide Reductase Beta 2 by Selective Cysteine Labeling with a Radical Phototrigger. *Proc. Natl. Acad. Sci.* **2012**, *109*, 39–43.

(15) Marcus, R. A. On the Theory of Oxidation-Reduction Reactions Involving Electron Transfer .1. *J. Chem. Phys.* **1956**, *24*, 966–978.

(16) Marcus, R. A. Chemical + Electrochemical Electron-Transfer Theory. *Annu. Rev. Phys. Chem.* **1964**, *15*, 155.

(17) Marcus, R. A. Electron-Transfer Reactions in Chemistry - Theory and Experiment. *Rev. Mod. Phys.* **1993**, *65*, 599–610.
(18) Marcus, R. A. Electron Transfer Past and Future. In *Electron transfer - from isolated molecules to biomolecules, PT 2*; Advances in Chemical Physics; 1999; Vol. 106, pp. 1–6.
(19) Gray, H. B.; Winkler, J. R. Long-Range Electron Transfer. *Proc. Natl. Acad. Sci.* **2005**, *102*, 3534–3539.
(20) Shih, C.; Museth, A. K.; Abrahamsson, M.; Blanco-Rodríguez, A. M.; Di Bilio, A. J.; Sudhamsu, J.; Crane, B. R.; Ronayne, K. L.; Towrie, M.; Vlček, Jr., A.; Richards, J. H.; Winkler, J. R., Gray, H. B. Tryptophan-Accelerated Electron Flow Through Proteins. *Science* **2008**, *320*, 1760–1762.
(21) Blanco-Rodríguez, A. M.; Busby, M.; Gradinaru, C.; Crane, B. R.; Di Bilio, A. J.; Matousek, P.; Towrie, M.; Leigh, B. S.; Richards, J. H.; Vlček Jr., A.; Gray, H. B. Excited-State Dynamics of Structurally Characterized [Re(I)(CO)3(phen)(HisX)]+ (X=83, 109) Pseudomonas Aeruginosa Azurins in Aqueous Solution. *J. Am. Chem. Soc.* **2006**, *128*, 4365–4370.
(22) Warren, J. J.; Ener, M. E.; Vlček Jr., A.; Winkler, J. R.; Gray, H. B. Electron Hopping through Proteins. *Coord. Chem. Rev.* **2012**, *256*, 2478–2487.
(23) Takematsu, K.; Williamson, H.; Blanco-Rodríguez, A. M.; Sokolová, L.; Nikolovski, P.; Kaiser, J. T.; Towrie, M.; Clark, I. P.; Vlček, Jr., A.; Winkler, J. R.; Gray, H. B. Tryptophan-Accelerated Electron Flow Across a Protein-Protein Interface. *J. Am. Chem. Soc.* **2013**, *135*, 15515–15525.
(24) Pascher, T.; Karlsson, B. G.; Nordling, M.; Malmström, B. G.; Vänngård, T. Reduction Potentials and Their pH Dependence in Site-Directed-Mutant Forms of Azurin from Pseudomonas Aeruginosa. *Eur. J. Biochem.* **1993**, *212*, 289–296.
(25) Skourtis, S. S.; Waldeck, D. H.; Beratan, D. N. Fluctuations in Biological and Bioinspired Electron-Transfer Reactions. **2010**, *61*, 461–485.
(26) Beratan, D. N.; Onuchic, J. N.; Winkler, J. R.; Gray, H. B. Electron-Tunneling Pathways in Proteins. *Science* **1992**, *258*, 1740–1741.
(27) Onuchic, J. N.; Beratan, D. N.; Winkler, J. R.; Gray, H. B. Pathway Analysis of Protein Electron-Transfer Reactions. *Annu. Rev. Biophys. Biomol. Struct.* **1992**, *21*, 349–377.
(28) Walden, S. E.; Wheeler, R. A. Distinguishing Features of Indolyl Radical and Radical Cation: Implications for Tryptophan Radical Studies. *J. Phys. Chem.* **1996**, *100*, 1530–1535.
(29) Beratan, D. N.; Onuchic, J. N. Electron-Tunneling Pathways in Proteins - Influences on the Transfer Rate. *Photosynth. Res.* **1989**, *22*, 173–186.
(30) Beratan, D. N.; Betts, J. N.; Onuchic, J. N. Protein Electron-Transfer Rates Set by the Bridging Secondary and Tertiary Structure. *Science* **1991**, *252*, 1285–1288.
(31) Balabin, I. A.; Onuchic, J. N. A New Framework for Electron-Transfer Calculations - Beyond the Pathways-like Models. *J. Phys. Chem. B* **1998**, *102*, 7497–7505.

(32) Regan, J. J.; Onuchic, J. N. Electron-Transfer Tubes. In *Electron transfer - from isolated molecules to biomolecules, PT 2*; Advances in Chemical Physics; 1999; Vol. 107, pp. 497–553.
(33) Skourtis, S. S.; Beratan, D. N. High and Low Resolution Theories of Protein Electron Transfer. *J. Biol. Inorg. Chem.* **1997**, *2*, 378–386.
(34) Ponce, A.; Gray, H. B.; Winkler, J. R. Electron Tunneling through Water: Oxidative Quenching of Electronically Excited Ru(tpy)(2)(2+) (tpy=2,2':6,2"-Terpyridine) by Ferric Ions in Aqueous Glasses at 77K. *J. Am. Chem. Soc.* **2000**, *122*, 8187–8191.
(35) Weidemaier, K.; Tavernier, H. L.; Swallen, S. F.; Fayer, M. D. Photoinduced Electron Transfer and Geminate Recombination in Liquids. *J. Phys. Chem. A* **1997**, *101*, 1887–1902.
(36) Villahermosa, R. Thesis, California Institute of Technology: Pasadena, California, 2002.
(37) Oevering, H.; Paddon-Row, M. N.; Heppener, M.; Oliver, A. M.; Cotsaris, E.; Verhoeven, J. W.; Hush, N. S. Long-Range Photoinduced through-Bond Electron-Transfer and Radiative Recombination via Rigid Nonconjugated Bridges - Distance and Solvent Dependence. *J. Am. Chem. Soc.* **1987**, *109*, 3258–3269.
(38) Stubbe, J.; Nocera, D. G.; Yee, C. S.; Chang, M. C. Y. Radical Initiation in the Class I Ribonucleotide Reductase: Long-Range Proton-Coupled Electron Transfer? *Chem. Rev.* **2003**, *103*, 2167–2201.
(39) Andrew, S. M.; Thomasson, K. A.; Northrup, S. H. Simulation of Electron-Transfer Self-Exchange in Cytochrome c and Cytochrome b5. *J. Am. Chem. Soc.* **1993**, *115*, 5516–5521.
(40) McLendon, G.; Miller, J. R. The Dependence of Biological Electron Transfer Rates on Exothermicity. the Cytochrome C/cytochrome b5 Couple. *J. Am. Chem. Soc.* **1985**, *107*, 7811–7816.
(41) Di Bilio, A. J.; Hill, M. G.; Bonander, N.; Karlsson, B. G.; Villahermosa, R. M.; Malmström, B. G.; Winkler, J. R.; Gray, H. B. Reorganization Energy of Blue Copper: Effects of Temperature and Driving Force on the Rates of Electron Transfer in Ruthenium- and Osmium-Modified Azurins. *J. Am. Chem. Soc.* **1997**, *119*, 9921–9922.
(42) Skov, L. K.; Pascher, T.; Winkler, J. R.; Gray, H. B. Rates of Intramolecular Electron Transfer in Ru(bpy)2(im)(His83)-Modified Azurin Increase below 220 K. *J. Am. Chem. Soc.* **1998**, *120*, 1102–1103.
(43) Di Bilio, A. J.; Dennison, C.; Gray, H. B.; Ramirez, B. E.; Sykes, A. G.; Winkler, J. R. Electron Transfer in Ruthenium-Modified Plastocyanin. *J. Am. Chem. Soc.* **1998**, *120*, 7551–7556.
(44) Babini, E.; Bertini, I.; Borsari, M.; Capozzi, F.; Luchinat, C.; Zhang, X.; Moura, G. L. C.; Kurnikov, I. V.; Beratan, D. N.; Ponce, A.; Di Bilio, A. J.; Winkler, J. R.; Gray, H. B. Bond-Mediated Electron Tunneling in Ruthenium-Modified High-Potential Iron-Sulfur Protein. *J. Am. Chem. Soc.* **2000**, *122*, 4532–4533.
(45) Moser, C. C.; Keske, J. M.; Warncke, K.; Farid, R. S.; Dutton, P. L. Nature of Biological Electron Transfer. *Nature* **1992**, *355*, 796–802.

(46) Merenyi, G.; Lind, J.; Shen, X. H. Electron-Transfer from Indoles, Phenol, and Sulfite (SO-3(-2)) to Chlorine Dioxide (ClO2). *J. Phys. Chem.* **1988**, *92*, 134–137.
(47) Huvaere, K.; Skibsted, L. H. Light-Induced Oxidation of Tryptophan and Histidine. Reactivity of Aromatic N-Heterocycles toward Triplet-Excited Flavins. *J. Am. Chem. Soc.* **2009**, *131*, 8049–8060.
(48) Harriman, A. Further Comments on the Redox Potentials of Tryptophan and Tyrosine. *J. Phys. Chem.* **1987**, *91*, 6102–6104.
(49) Warren, J. J.; Winkler, J. R.; Gray, H. B. Redox Properties of Tyrosine and Related Molecules. *FEBS Lett.* **2012**, *586*, 596–602.
(50) Creutz, C.; Chou, M.; Netzel, T. L.; Okumura, M.; Sutin, N. Lifetimes, Spectra, and Quenching of the Excited States of Polypyridine Complexes of Iron(II), Ruthenium(II), and Osmium(II). *J. Am. Chem. Soc.* **1980**, *102*, 1309–1319.
(51) Sutin, N.; Creutz, C. Properties and Reactivities of the Luminescent Excited States of Polypyridine Complexes of Ruthenium(II) and Osmium(II). In *Inorganic and Organometallic Photochemistry*; Advances in Chemistry; American Chemical Society: Washington, DC, 1978; Vol. 1.
(52) Battistuzzi, G.; Bellei, M.; Bortolotti, C. A.; Sola, M. Redox Properties of Heme Peroxidases. *Arch. Biochem. Biophys.* **2010**, *500*, 21–36.
(53) Green, M. T.; Dawson, J. H.; Gray, H. B. Oxoiron(IV) in Chloroperoxidase Compound II Is Basic: Implications for P450 Chemistry. *Science* **2004**, *304*, 1653–1656.